EURASIP Journal on Advances in Signal Processing
a SpringerOpen Journal

RESEARCH Open Access

Low-complexity sparse reconstruction for high-resolution multi-static passive SAR imaging*

Xinhua Mao[1,2], Yimin D Zhang[2*] and Moeness G Amin[2]

Abstract

Bi-static passive synthetic aperture radar (SAR) systems using ground broadcast and wireless network signals suffer from a low spatial resolution due to the narrow bandwidths and low carrier frequencies. By exploiting multiple distributed illuminators, multi-static passive radar has the possibility of producing high-resolution SAR images. In this paper, a two-stage image formation approach, which combines the Fourier transform and sparse reconstruction strategies, is proposed to process multi-static SAR data. This method exploits the group sparsity of the sparse scene, i.e., the observations associated with different bi-static pairs share the same support of the sparse scene but correspond to aspect-dependent scattering coefficients. Such observations are described as a number of generally disjoint sub-bands in the two-dimensional spatial frequency domain. In each sub-band, the sampling satisfies the Nyquist criterion, whereas different sub-bands are sparsely distributed. In the proposed approach, Fourier-based reconstruction is applied to the sub-band data to produce the coarse-resolution images, which are then combined to produce a high-resolution image through the exploitation of sparse reconstruction techniques. The proposed approach greatly improves the imaging quality as compared to Fourier-based reconstruction, whereas it exhibits significant reduction of the computational complexity when compared to direct application of sparse reconstruction techniques. The exploitation of block sparsity-based techniques also permits practical treatment of the angle-dependent target scattering characteristics in SAR image reconstruction. The advantages of the proposed approach are delineated using analysis and simulations.

1 Introduction

Passive radar encompasses a class of radar systems that detect and track objects by processing reflections from noncooperative illumination sources of opportunity in the environment, such as commercial broadcast and communications signals [1-3]. Due to the inherent narrow signal bandwidth and low carrier frequency properties of the transmitted signals, passive radar often suffers from low spatial resolution [4][a]. This makes object identification a challenging problem. Multi-static passive synthetic aperture radar (SAR) employs multiple physical transmitters and a moving receiver with a synthetic array aperture to provide a higher number of independent measurements and hence enables high-resolution image formations. From a tomographic perspective, the collected data reflected from the scene provide samples of the Fourier transform of the reflectivity of the target in the two-dimensional (2-D) spatial frequency (wavenumber) domain [5]. Therefore, SAR image formation can be considered as an image reconstruction from its Fourier-sampled data.

In the literatures, there are two types of algorithms that produce image from Fourier samples. One is based on classical linear reconstruction techniques, such as backprojection [6,7] and direct Fourier reconstruction [8,9]. These algorithms are scene-independent and, therefore, widely used in practical applications due to their simplicity. They, however, require that the data are sampled at the Nyquist rate. When the data are undersampled or otherwise missing samples are present, the system is underdetermined from the linear reconstruction viewpoint. In this respect, the resulting image suffers from undesired artifacts and high sidelobes.

To solve this problem, nonlinear reconstruction techniques, particularly sparse reconstruction or compressive sensing, have been proposed in recent years [10,11]. Sparse reconstruction can accurately reconstruct a sparse scene with very fewer Fourier samples, provided that the restricted isometry property (RIP) is satisfied [12,13]. Improved SAR imaging is achieved by using the

* Correspondence: yimin.zhang@villanova.edu
[2]Center for Advanced Communications, Villanova University, 800 E, Lancaster Ave., Villanova, PA 19085, USA
Full list of author information is available at the end of the article

sparse Bayesian learning algorithms that are based on relevance vector machine [14,15]. Such techniques, however, may become difficult to implement for processing a large scene because of the very high dimension of the associated dictionary matrix.

In this paper, we propose a hybrid SAR imaging technique that combines the Fourier transform-based approach with the group sparse signal reconstruction methods [16]. As such, the proposed technique achieves high-resolution imaging with a significantly lower computation costs. We first demonstrate the block sparsity of the Fourier domain samples in a multi-static passive SAR. That is, the Fourier sampling patterns contain a number of generally disjoint sub-bands in the 2-D spatial frequency domain. In each sub-band, the sampling satisfies the Nyquist criterion, whereas different sub-bands are sparsely distributed. By exploiting this property, we propose a two-stage image formation approach which combines the Fourier-based imaging and sparse signal reconstruction strategies. Since the sampling satisfies the Nyquist criterion in each sub-band, Fourier-based reconstruction is applied to produce the coarse-resolution images, which are then combined to produce a high-resolution image through the exploitation of group sparse reconstruction techniques. Because the final SAR image is constructed through sparse signal reconstruction, the proposed approach can avoid the artifact effect in Fourier-based reconstructions due to disjoint and sparse sub-bands. On the other hand, because the sparse construction is separately applied to segmented scene areas, it exhibits significant reduction of the computational complexity when compared to direct sparse reconstruction. The exploitation of group sparsity-based techniques also permits practical treatment of the angle dependency of the scattering characteristics in SAR image construction.

The remainder of this paper is organized as follows: Section 2 presents the signal model for multi-static passive SAR; in Section 3, we examine the relationship between radar performance and radar configurations; in Section 4, a two-stage image formation algorithm is proposed to perform multi-static SAR imaging; and finally, in Section 5, we validate the effectiveness of the proposed approach by simulation experiments.

2 Multi-static passive SAR

In this section, we first introduce the tomographic interpretation for a bi-static passive radar pair and then extend the model to a multi-static radar case.

2.1 Bi-static radar

Consider a bi-static radar data collection geometry as shown in Figure 1a. For the clarity of analyses, we consider the 2-D geometry without loss of generality, but the results can be easily extended to the 3-D case. In this geometry, the center of the interested scene is defined as the origin of coordinate system, while the positions of transmitter and receiver are determined by their polar radius and polar angle, i.e., $[r_{\mathrm{Tc}}, \theta_{\mathrm{T}}]$ and $[r_{\mathrm{Rc}}, \theta_{\mathrm{R}}]$, respectively. We assume that an arbitrary point target is located in the scene with coordinate (x_t, y_t), and its scattering coefficient is σ. The ranges from the transmitter and receiver to the target are denoted by r_{T} and r_{R}, respectively.

Let the transmitter emit signal $s(\tau) = \exp(i2\pi f\tau)$ to illuminate the service area. The receiver receives the signal scattered from the target. After demodulation, the received signal can be expressed as

$$r(\tau) = \sigma \cdot \exp\left[-i2\pi f \frac{r_{\mathrm{T}} + r_{\mathrm{R}}}{c}\right], \tag{1}$$

where c is the velocity of light.

After motion compensation to the scene center, it becomes

$$\hat{r}(\tau) = \sigma \cdot \exp\left[i2\pi f \frac{r_{\mathrm{Tc}} + r_{\mathrm{Rc}} - r_{\mathrm{T}} - r_{\mathrm{R}}}{c}\right]. \tag{2}$$

Assume that the target point is close to the scene origin and that transmitter and receiver are in the far field region of the scene. In this case, the wave front is planar and (2) can be written as

$$\begin{aligned}\hat{r}(\tau) &= \sigma \cdot \exp\left\{i\frac{2\pi f}{c}\left[x_t(\cos\theta_{\mathrm{T}} + \cos\theta_{\mathrm{R}}) + y_t(\sin\theta_{\mathrm{T}} + \sin\theta_{\mathrm{R}})\right]\right\} \\ &= \sigma \cdot \exp\left[i\left(x_t k_x + y_t k_y\right)\right],\end{aligned} \tag{3}$$

where

$$\begin{aligned} k_x &= \frac{2\pi f}{c}(\cos\theta_{\mathrm{T}} + \cos\theta_{\mathrm{R}}) \\ k_y &= \frac{2\pi f}{c}(\sin\theta_{\mathrm{T}} + \sin\theta_{\mathrm{R}}) \end{aligned} \tag{4}$$

are the spatial frequencies in the x and y directions, respectively. They can also be conveniently expressed in the polar format:

$$\begin{aligned} k_r &= \sqrt{k_x^2 + k_y^2} = \frac{4\pi f}{c}\cos\left(\frac{\theta_{\mathrm{T}} - \theta_{\mathrm{R}}}{2}\right), \\ \theta_b &= a\tan\left(\frac{k_y}{k_x}\right) = a\tan\left(\frac{\sin\theta_{\mathrm{T}} + \sin\theta_{\mathrm{R}}}{\cos\theta_{\mathrm{T}} + \cos\theta_{\mathrm{R}}}\right) = \frac{\theta_{\mathrm{T}} + \theta_{\mathrm{R}}}{2}. \end{aligned} \tag{5}$$

From (3), it is clear that the data after preprocessing, i.e., $\hat{r}(\tau)$, is essentially a sample in the wavenumber domain of the target. The sample position is determined by the azimuth angles of the transmitter/receiver and the frequency of transmitted signal. As illustrated in Figure 1, the azimuth angle of the transmitter and the signal frequency respectively determine the position and size of

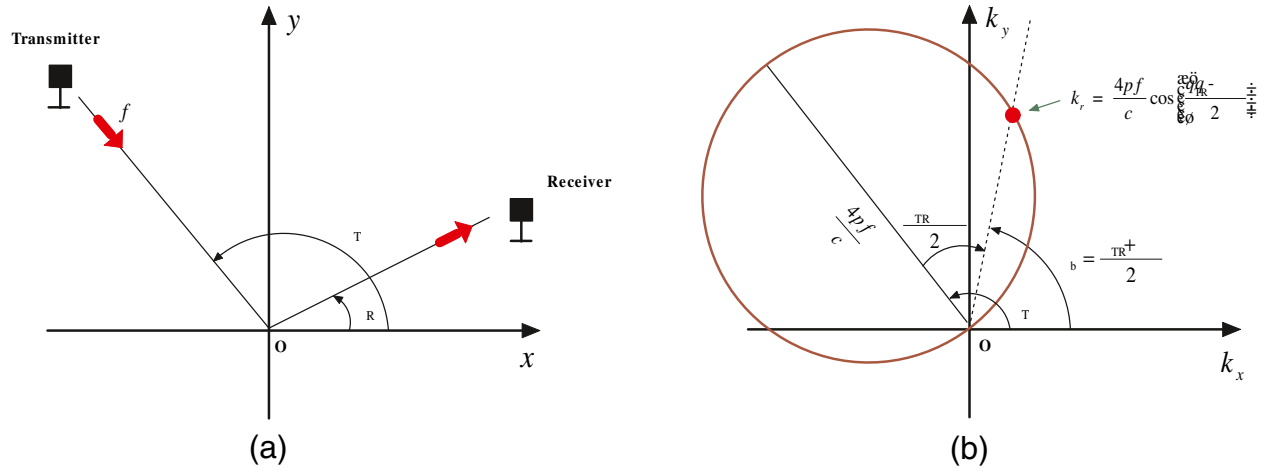

Figure 1 Data collection geometry and sample position in the wavenumber domain for a bi-static radar. (a) Data collection geometry. **(b)** Sample position in wavenumber domain.

the red circle, whereas the azimuth angles of the transmitter and receiver determine the dash line. Then, the sample position is the intersection of the red circle and the dash line.

2.2 Multi-static passive SAR

From the above analysis, we know that the data collected by an individual bi-static radar pair with a single frequency illuminator provide a single sample in the wavenumber domain. For a general multi-static passive SAR where multiple transmitters and/or receivers are used, we can obtain different samples in the wavenumber domain due to space and frequency diversity. They provide the opportunity to reconstruct the scene with an improved resolution. The respective offerings of multiple transmitter and receivers are summarized below.

2.2.1 Transmitter diversity

Multi-static passive radar with multiple transmitters can provide both space diversity and frequency diversity. In general, a passive radar uses multiple spatially separated commercial illuminators of opportunity as the transmitters. The observations from different directions by exploiting these different illuminators can provide the space diversity, whereas the frequency diversity in multi-static passive radar is achieved as these illuminators are usually operated at different carrier frequencies.

2.2.2 Receiver diversity

Multiple apertures located at different positions can provide space diversity. These multiple apertures can be either physical or synthetic. For airborne radar, typically for SAR, the synthetic apertures can be obtained by exploiting the motion of platform.

Now, we consider the signal model in the multi-static passive radar. Without loss of generality, we assume J illuminators, each being operated at a different carrier frequency. We assume that the jth illuminator transmits a signal with bandwidth B_j and carrier frequency f_{cj}. The airborne receiver receives the scattered echo from the scene at a constant repeat time interval. During the coherent processing interval (CPI) corresponding to an accumulated angle $\Delta\theta$, it collects K sample sets at K different azimuth positions. Each sample set contains the scene echo corresponding to the J illuminators. Because different carrier frequencies are used, the echo corresponding each illuminator can be separated. From (3), we obtain the signal model for multi-static SAR as

$$\begin{aligned} r(j,k,l) &= \sigma\cdot\exp\left\{ i\frac{2\pi\left(f_{cj}+f_l\right)}{c}\left[x_t\left(\cos\theta_{Tj}+\cos\theta_{Rk}\right)+y_t\left(\sin\theta_{Tj}+\sin\theta_{Rk}\right)\right]\right\} \\ &= \sigma\cdot\exp\left\{ i\left[x_t k_x^{jkl}+y_t k_y^{jkl}\right]\right\}, \end{aligned} \tag{6}$$

where θ_{Tj} is the azimuth angle of the jth illuminator; f_l is the lth sample frequency in the range of signal bandwidth, $l = 1,\cdots, L$; and θ_{Rk} is the azimuth angle of the receiver at the kth receive interval. In addition, $k_x^{jkl} = \frac{2\pi\left(f_{cj}+f_l\right)}{c}\left(\cos\theta_{Tj}+\cos\theta_{Rk}\right)$ and $k_y^{jkl} = \frac{2\pi\left(f_{cj}+f_l\right)}{c}\left(\sin\theta_{Tj}+\sin\theta_{Rk}\right)$ represent the spatial frequencies in the x and y directions, respectively.

Due to space and frequency diversity, i.e., the variation of f_{cj}, f_l, θ_{Tj}, and θ_{Rk}, the data collected by the airborne multi-static SAR represent multiple samples in the wavenumber domain. Typically, the samples with respect to f_l and θ_{Rk} are dense and satisfy the Nyquist sample requirement, whereas the samples are often sparse with

respect to f_{cj} and θ_{Tj}. Therefore, the sample support of wavenumber domain is often block sparse. This property is intuitively illustrated in Figure 2. Specifically, Figure 2a shows the geometry of a multi-static passive radar configuration, and Figure 2b depicts the corresponding sample support pattern.

3 Radar configuration and system performance

The performance of sparse scene SAR imaging depends on the available degrees of freedom (DOFs) of the radar system and the scene sparsity. A high number of DOFs yield an improved resolution of the sparse scene. For a band-limited signal, the number of DOFs is proportional to the product of its time-domain duration and frequency-domain bandwidth [17]. For a constant time-domain duration, the number of DOFs is proportional only to the size of frequency-domain support.

For the multi-static passive SAR, it is desirable to increase the area of frequency-domain support in order to achieve a good scene resolution. Toward this end, we need to understand how the frequency-domain support is determined by the radar parameters. We first consider a single illuminator case and assume the frequency range of the emitted signal to be $[f_c, f_c + B]$. The accumulative angle of the receiver during the CPI is $\Delta\theta$, and the corresponding bi-static angle ranges from $2\theta_{bc} - \frac{\Delta\theta}{2}$ to $2\theta_{bc} + \frac{\Delta\theta}{2}$.

According to the geometry depicted in Figure 2, the size of support pattern is obtained as

$$S = \frac{4\pi^2}{c^2}\left[\Delta\theta + 2\sin\frac{\Delta\theta}{2}\cos(2\theta_{bc})\right]\left(f_c + \frac{B}{2}\right)B. \qquad (7)$$

It is clear from (7) that broadening of the wavenumber domain support area can be achieved by exploiting the frequency diversity (due to bandwidth B) and the space diversity (due to accumulative angle $\Delta\theta$). Therefore, to increase the size of the wavenumber domain support area, a direct way is to select the illuminators with a high signal bandwidth and/or to increase the coherent accumulative angle of the receiver. We also observe from (7) that the carrier frequency of transmitted signal and the bi-static angle also affect the size of support area. A higher carrier frequency results in a larger support area, provided that the bi-static angles remain the same. That is, whenever possible, it is desirable to choose the illuminators which are operated in higher carrier frequencies. In addition, a small bi-static angle will result in a large support area. In the extreme case, the support area achieves its maximum value in the mono-static case, i.e., when the bi-static angle is zero,

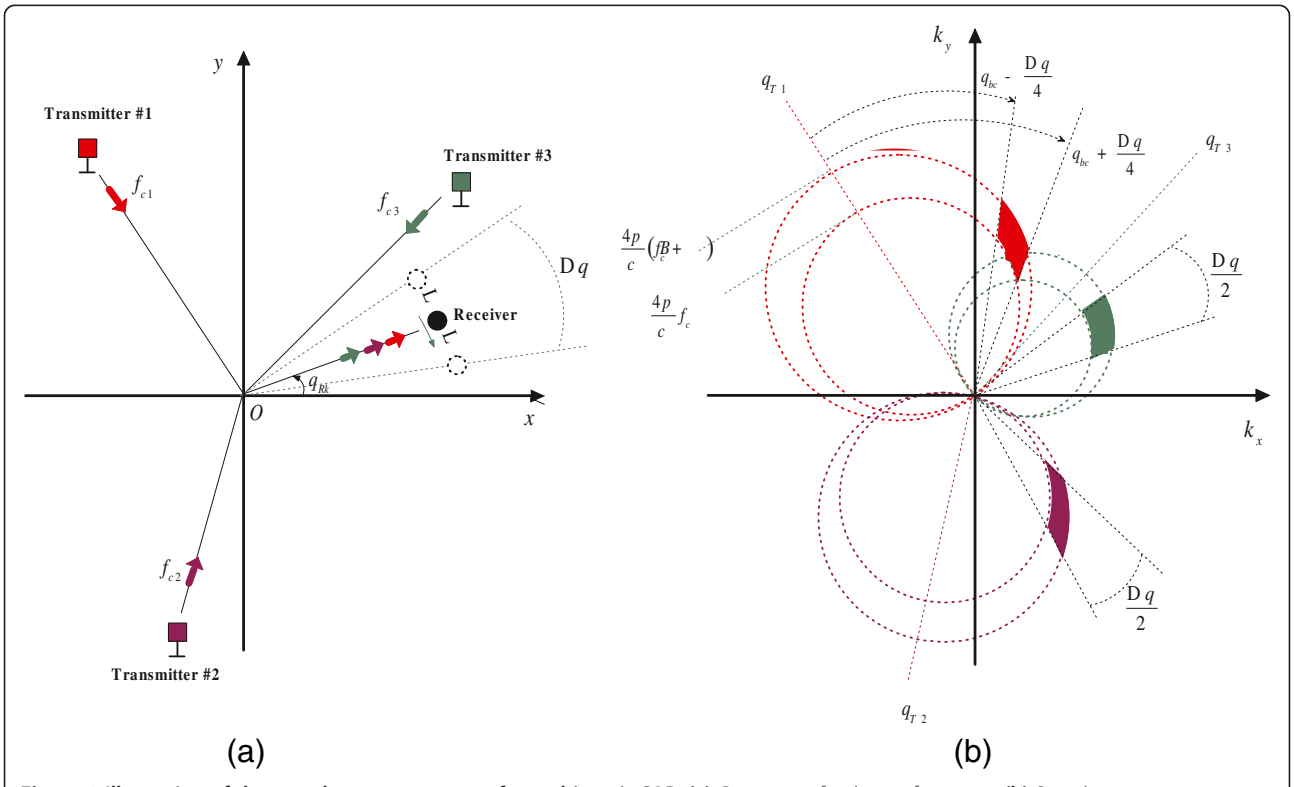

Figure 2 Illustration of the sample support pattern for multi-static SAR. (a) Geometry of radar configuration. **(b)** Sample support pattern in wavenumber domain.

whereas it reaches its minimum value when the bi-static angle is 180° ($\theta_{bc} = 90°$).

When multiple illuminators are used for multi-static passive SAR, the total observation area provided by the multi-static SAR is the superposition of the sub-observation areas provided by all the available bi-static pairs. From the point of view of Fourier reconstruction, it is desirable that all the sub-observation areas be seamlessly mosaicked into a large and connected area. However, this rarely occurs in actual situations because the illuminators are usually sparse and noncooperative. As a result, the multiple sub-observation areas are usually disjoint and sparsely distributed in the wavenumber domain.

Sparse distributions of the illuminators can benefit the space diversity effects, e.g., providing the capability to suppress the angular glint effect. However, their excessive sparse distributions may have an adverse impact on the high-resolution reconstruction. As discussed above, the support area in the frequency domain of an illuminator is closely related to the bi-static angle between the transmitter and the receiver. If the bi-static angle is very large, the corresponding support area becomes small, which is detrimental to the high-resolution reconstruction. For an airborne passive radar, the angle of the receiver usually varies in a small interval. Consequently, if the illuminators are excessively sparse, the bi-static angles in some illuminator-receiver pairs will become large and the corresponding wavenumber domain support area is reduced. For example, Figure 3 shows two different kinds of illuminator location configurations. In Figure 3a, the spatial distribution of the four illuminators is approximately uniform, whereas in Figure 3b, these illuminators are located much closer to the receiver. The wavenumber domain support areas corresponding to these two configurations are compared in Figure 4 for a passive SAR system with identical exemplar parameters. In Figure 4a, the total support area is 10.3354 $(\text{rad/m})^2$, whereas it becomes 17.6399 $(\text{rad/m})^2$ in Figure 4b. Obviously, the configuration corresponding to Figure 4b will have better reconstruction performance, provided that all other parameters are equal.

4 Image formation

For the multi-static passive radar, as discussed in the previous section, the wavenumber domain sample patterns are block sparse, i.e., the observed support areas are composed of a number of sparsely distributed sub-bands. Within each sub-band, the data are sampled at the Nyquist rate. Considering this specific sampling pattern, we propose a two-stage image formation algorithm, which combines the linear and nonlinear reconstruction techniques together. In the first-stage of image formation, we produce a series of coarse-resolution images separately from each sub-band data by using a linear reconstruction algorithm, since the sub-band data are Nyquistly sampled. In the second stage, the information extracted from the coarse-resolution images is exploited by a group sparse reconstruction technique to form an image with a finer resolution. Because the second stage is applied from coarse images

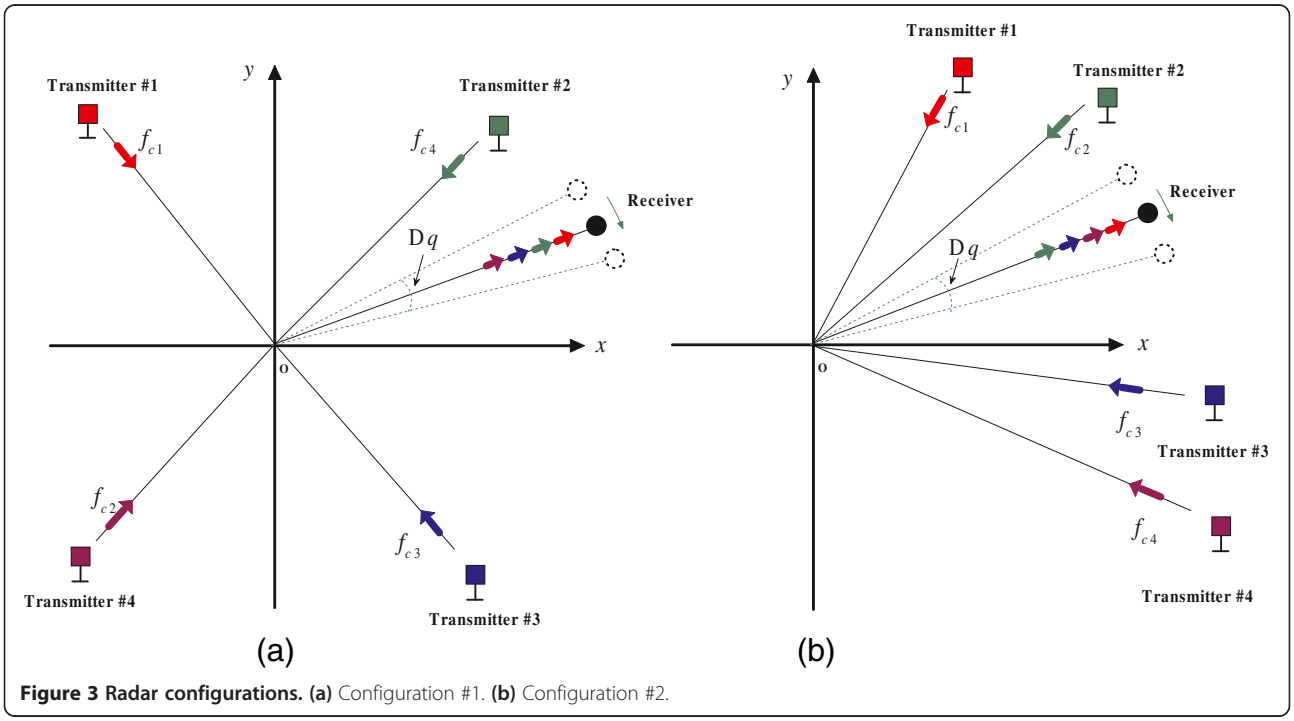

Figure 3 Radar configurations. (a) Configuration #1. **(b)** Configuration #2.

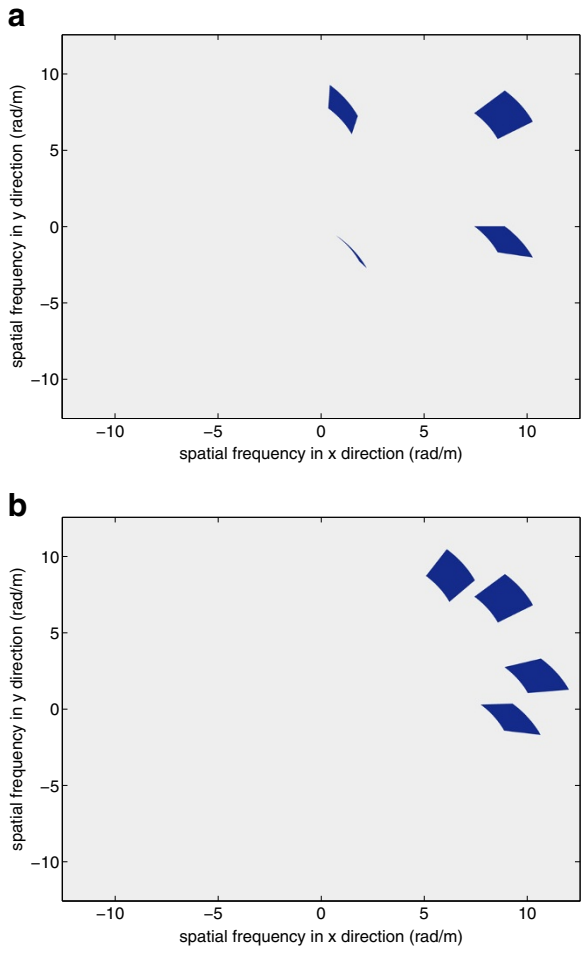

Figure 4 Wavenumber domain support area. (a) Corresponding to configuration #1. **(b)** Corresponding to configuration #2.

to form a fine image, it allows the group sparse reconstruction to be applied in segmented image areas so as to obtain high-resolution image quality with a low complexity. This two-stage processing strategy is illustrated in Figure 5 and is detailed below.

4.1 First-stage image formation

From (6), it is evident that the data in each sub-band are, in essence, group sparse samples of the 2-D Fourier transform of the terrain reflectivity. In general, the observed samples are uniformly spaced in the (f_l, θ_{Rk}) domain. They become nonuniformly spaced when they are mapped to the wavenumber domain (k_x, k_y). Therefore, to exploit the computationally efficient algorithms such as the fast Fourier transform (FFT), a 2-D interpolation of the sampled data onto a rectangular grid in the (k_x, k_y) domain is performed. This process is referred to as polar format transformation [17] and is illustrated in Figure 6.

After performing polar format transformation, the signal depicted in (6) can be expressed as

$$r(j,k,l) = \sigma \cdot \exp\left\{ i\left[x_t k_x^{jk} + y_t k_y^{jl} \right] \right\}, \tag{8}$$

where $k_x^{jk} = k_{xc}^{j} + \left(k - \frac{K}{2}\right)\Delta_{k_x}, k = 1, \cdots, K$ and $k_y^{jl} = k_{yc}^{j} + \left(l - \frac{L}{2}\right)\Delta_{k_y}, l = 1, \cdots, L$ are the resampled positions in the k_x and k_y domains, respectively. To facilitate the following processing, all the sub-band outputs are designed to share the same Cartesian coordinates but with different support centers. For the jth sub-band, the support center of the wavenumber domain is set as

$$\begin{aligned} k_{xc}^{j} &= \frac{2\pi f_{cj}}{c}\left(\cos\theta_{Tj} + \cos\theta_{Rc}\right), \; k_{yc}^{j} \\ &= \frac{2\pi f_{cj}}{c}\left(\sin\theta_{Tj} + \sin\theta_{Rc}\right) \end{aligned} \tag{9}$$

where θ_{Rc} is the nominal angle of the target observed from the receiver. Performing 2-D FFT on (8) yields a series of coarse-resolution images, expressed as

$$r(j,n,m) = \sigma \cdot A^{j}\left(\frac{n}{K\Delta_{k_x}} - x_t, \frac{m}{L\Delta_{k_y}} - y_t \right) \cdot \exp\left\{ i\left[x_t k_{xc}^{j} + y_t k_{yc}^{j} \right] \right\} \tag{10}$$

where $A^j(x, y)$ is the point spread function for the jth sub-band data, and $\frac{1}{K\Delta_{k_x}}$ and $\frac{1}{L\Delta_{k_y}}$ are the pixel sizes in the x and y directions, respectively.

From (10), we can obtain a coarse estimate of target position as

$$\hat{x}_t = \frac{n_0}{K\Delta_{k_x}}, \quad \hat{y}_t = \frac{m_0}{L\Delta_{k_y}} \tag{11}$$

whose respective accuracies are $\frac{1}{K\Delta_{k_x}}$ and $\frac{1}{L\Delta_{k_y}}$. In (11), n_0 and m_0 are the pixel indexes of the target location in the x and y directions, respectively.

4.2 Second-stage image formation

Because of the narrow signal bandwidth and small coherent accumulation angle, the image produced by each sub-band data often has a poor resolution. However, there are a number of such coarse-resolution images corresponding to the available illuminators. By coherently combining these sub-band images, therefore, the image resolution can be improved. If all the sub-band data had the same support and could be mosaicked seamlessly, performing another Fourier transform across the coarse-resolution sub-images would directly yield an image with a higher resolution. For the multi-static passive SAR, however, as discussed in the previous section, Fourier reconstruction may not yield desirable imaging performance with a high resolution and low sidelobes because the sub-bands are sparsely distributed in the wavenumber domain. In addition, to obtain the phase information

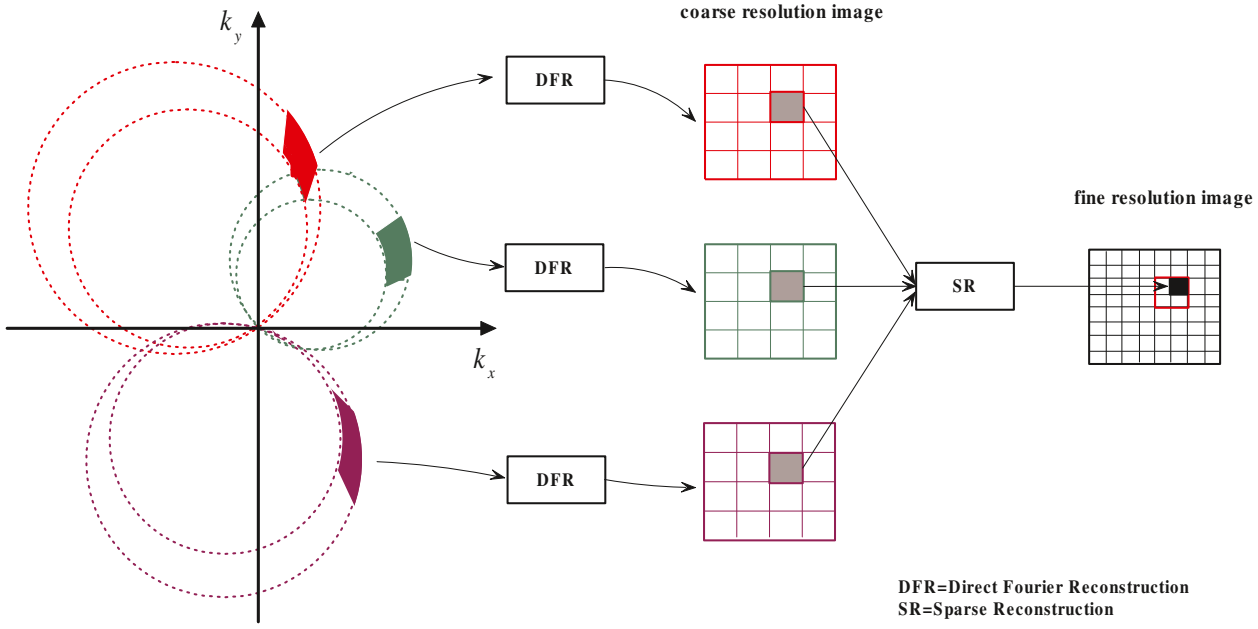

Figure 5 Illustration of the proposed two-stage image formation method.

underlying the Fourier reconstruction, one must assume that the target scattering coefficients are independent of the aspect of the illuminator. That is, the scattering coefficients must be invariant to the incident angles. As a matter of fact, however, the radar cross section (RCS) of most objects changes as a function of the aspect. When the illuminators are sparsely distributed in the aspect, therefore, the above assumption becomes invalid.

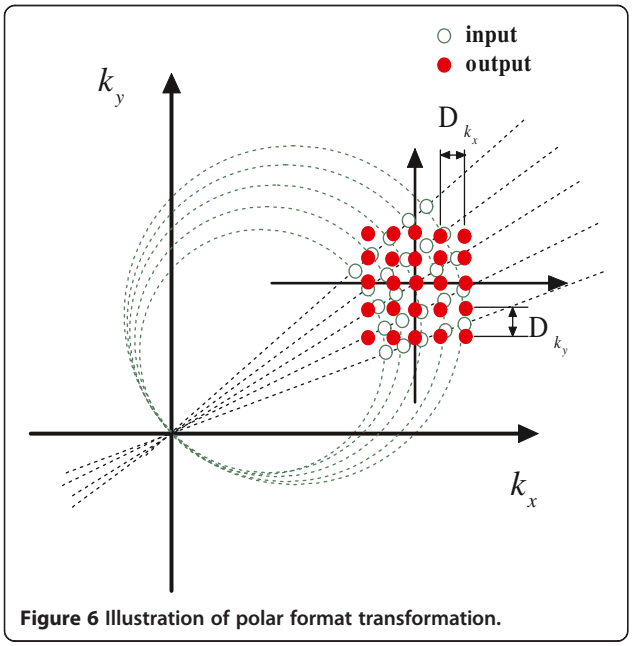

Figure 6 Illustration of polar format transformation.

In such situations, the recently developed nonlinear reconstruction techniques, i.e., sparse signal reconstruction and compressive sensing approaches, can provide an effective target reconstruction capability provided that the scene is sparse. Such sparse scene imaging problems to be considered herein are important in practice. In many real-world applications, the scene is itself strictly sparse or can be approximated with a small number of strong scatterers whereas the other weak scatterers can be considered insignificant. In addition, many nonsparse scenes can be considered as sparse in a transformed representation, such as the image edges. As such, in the sequel, we employ sparse reconstruction techniques in the second image formation stage to fuse the coarse-resolution images.

In this stage, each coarse-resolution image pixel is divided into $N \times N$ fine-resolution pixels. Therefore, the size of the new pixel in range and azimuth becomes $\frac{1}{NK\Delta_{k_x}}$ and $\frac{1}{NL\Delta_{k_y}}$, respectively. For the jth illuminator, the signals at the coarse-resolution cell and the fine-resolution cell can be associated by a transform matrix, expressed as

$$r^{(j)} = \Phi^{(j)} w^{(j)}, j = 1, 2, \cdots, J, \tag{12}$$

where $r^{(j)}$ is the value of the pixel generated in the coarse-resolution image, $w^{(j)} = \left[w_1^j, \cdots, w_{N^2}^j\right]^T$ is the fine-resolution pixel vector to be reconstructed. In addition, $\Phi^{(j)}$

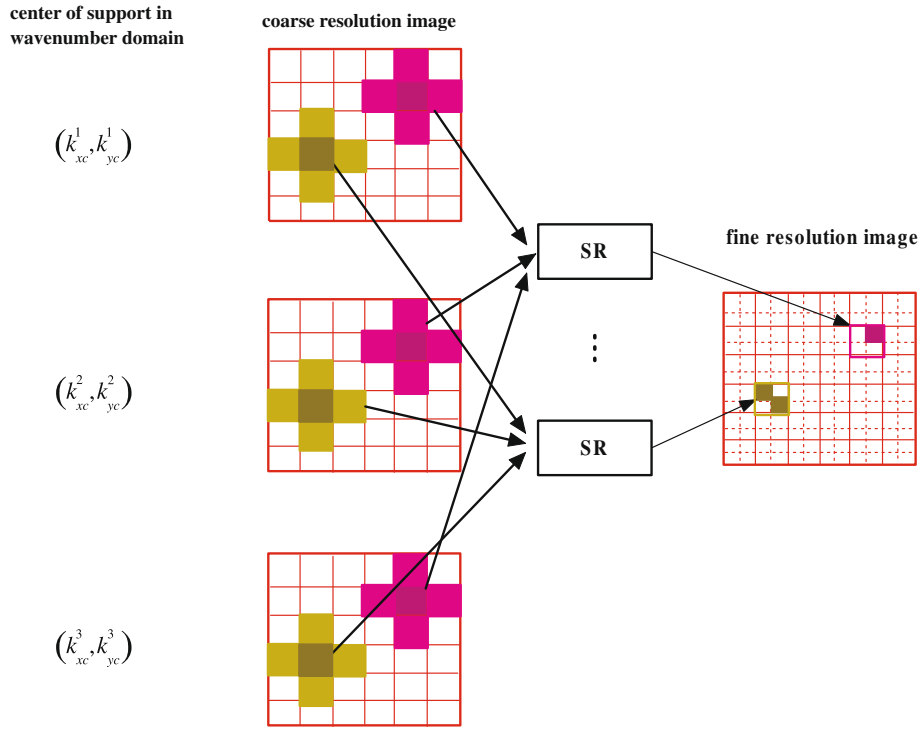

Figure 7 Illustration of sparse reconstruction in the second stage.

is the sensing row vector of size $1 \times N^2$, whose element located in the nth column can be expressed as

$$\phi_n^{(j)} = A^j(x_c - x_n, y_c - y_n) \cdot \exp\left\{ i\left[x_n k_{xc}^j + y_n k_{yc}^j \right] \right\}, \quad (13)$$

where (x_c, y_c) is the coordinate of the coarse-resolution pixel cell and (x_n, y_n) is the coordinate of the nth fine-resolution pixel in the coarse-resolution cell.

Because of the spreading effects of a point target in the Fourier-based reconstruction, which can be described as the extent of the point spread function, the scattering from a point target contributes to the coarse-resolution image not only at its true position but also at the neighboring pixels. Such point spreading effects are not fully accounted for if we construct the fine-resolution images based on each coarse-resolution pixel alone and, as a result, will degrade the quality of the resulting fine-resolution image in two aspects: on one hand, the interference from scatterers of the neighboring coarse-resolution pixels cannot be efficiently mitigated, and on the other hand, the observations made in the neighboring coarse-resolution pixels are not fully utilized for the fine-image construction in the underlying coarse-resolution pixel. Therefore, it is desirable to exploit multiple coarse-resolution pixels to construct the fine-resolution images in the second stage. The size of pixel region should be consistent with the point spreading function such that the point spreading function corresponding to each point target takes insignificant values outside this region. A more detailed discussion about the pixel region selection is addressed in [18]. Toward this end, we modify (12) by using Q coarse-resolution pixels, and the expression is given by

$$\tilde{r}^{(j)} = \tilde{\Phi}^{(j)} \tilde{w}^{(j)}, j = 1, 2, \cdots, J, \quad (14)$$

where $\tilde{r}^{(j)} = \left(r_1^j, \cdots, r_Q^j \right)^T$ is a vector containing the values of Q selected neighboring coarse-resolution pixels, $\tilde{w}^{(j)}$ represents a vector of the unknown fine-resolution pixels

Table 1 Frequencies and azimuth angles of the eight illuminators

Illuminator	f_c (MHz)	Azimuth angle (degree)
1	450	5
2	570	10
3	510	45
4	480	25
5	660	30
6	540	20
7	630	15
8	600	50

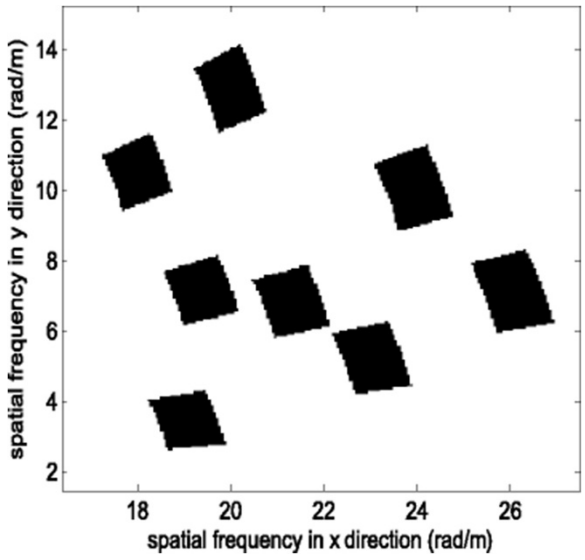

Figure 8 Support area in the wavenumber domain.

contained in the Q coarse-resolution pixels, and $\widetilde{\Phi}^{(j)}$ is a $Q \times QN^2$ sensing matrix, whose (q,n)th element is

$$\phi_{q,n}^{(j)} = A^j\left(x_q - x_n, y_q - y_n\right) \cdot \exp\left\{i\left[x_n k_{xc}^j + y_n k_{yc}^j\right]\right\}, \tag{15}$$

with (x_q, y_q) denoting the position of the qth coarse-resolution pixel.

As we described earlier, in multi-static passive SAR, the scattering coefficients of a fine-resolution pixel differ with respect to different illuminators due to their different aspect angles. That is, the fine-resolution pixel coefficients

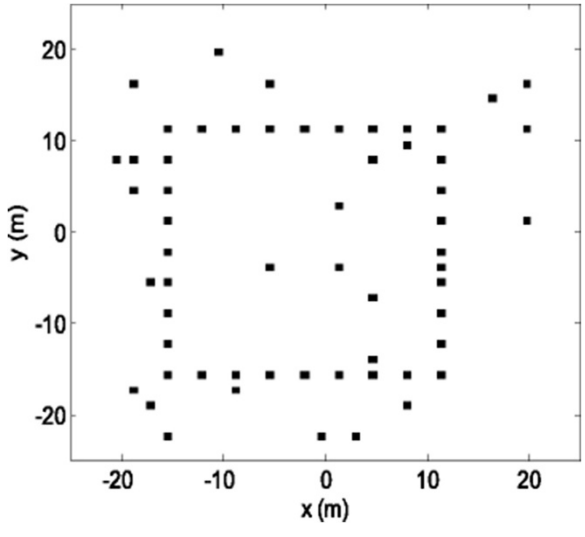

Figure 9 Target locations in the scene.

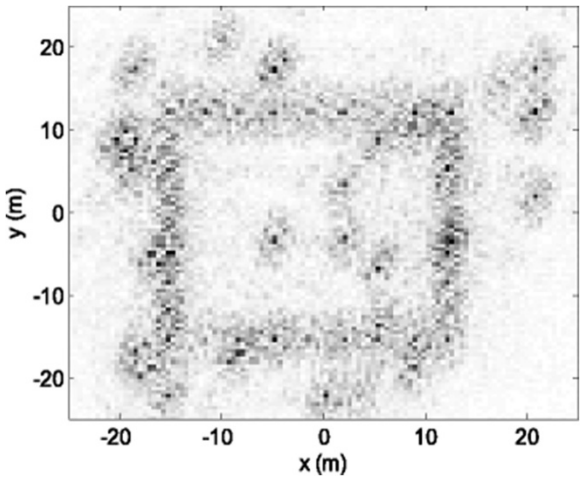

Figure 10 Image produced by direct Fourier reconstruction.

to be estimated, which are expressed as vectors $\widetilde{w}^{(j)}$ in (14), are modeled to be independent for different index j. Nevertheless, because the same sparse scatterers contribute to the observations corresponding to the different illuminators, the positions of the nonzero entries in the vectors $\widetilde{w}^{(j)}$ are identical or highly overlap. This characteristic is referred to as the block sparsity or group sparsity [19], which can be effectively solved using techniques that take such property into account. Such group sparsity solvers include block sparsity-based compressed sensing [20], multi-task Bayesian compressed sensing [21,22], and distributed compressed sensing [23].

Equation (14) is solved for each coarse-resolution pixel and repeated until all the coarse-resolution pixels are processed. Finally, all the obtained fine-resolution sub-images are mosaicked to obtain the high-resolution

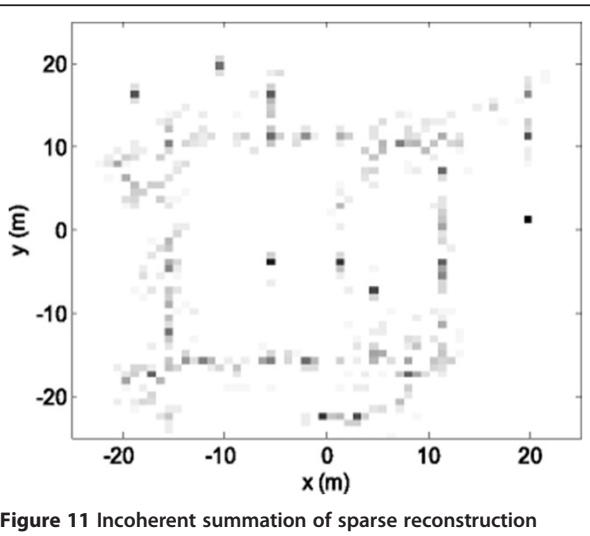

Figure 11 Incoherent summation of sparse reconstruction image for multiple illuminators.

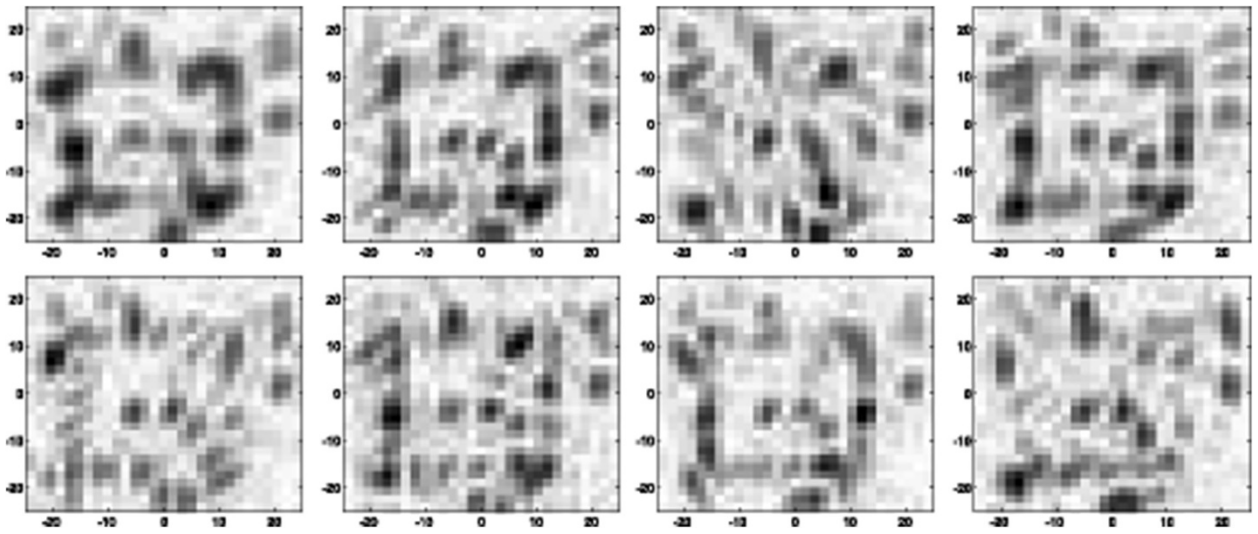

Figure 12 Eight coarse-resolution images produced by the first-stage processing.

image of the entire scene. The proposed second-stage processing is illustrated in Figure 7. Note that, while the fine-resolution pixel coefficients are computed for Q coarse-resolution pixels each time, only the results obtained for the underlying coarse-resolution pixel are maintained and those belonging to the neighboring coarse-resolution pixels are discarded. This concept can be extended to process multiple pixels at once by extending the size of Q such that the contribution of the interested multiple pixels outside the Q pixel region is insignificant.

4.3 Computational complexity

The proposed sparse image reconstruction technique divides the SAR image reconstruction into two stages, and the first stage can be efficiently implemented using the FFT. As such, while enjoying the high quality of resulting images as the result of sparse signal reconstruction, the proposed technique achieves significant reduction of the computation complexity when compared with direct sparse image reconstruction from the observed data. In the following, a quantitative analysis is provided.

Consider a simple model where J illuminators are present and, for each of the emitted signals, we collect L samples in the frequency bandwidth dimension and K samples in azimuth angle dimension. As such, the total number of data samples is JLK. Also assume that the dimension of the fine-resolution image pixels to be constructed in the entire scene is $LN \times KN$. We consider that complexity of the direct sparse image recovery is proportional to the nth power of the dimension of the observation data and that of the scene pixels. The value of n depends on the reconstruction algorithms and usually varies between 2 and 3. As such, the computation complexity required for directly reconstructing image from the observed data is $(JKL \cdot LN \cdot KN)^n = J^n K^{2n} L^{2n} N^{2n}$. For the proposed two-stage imaging technique, the complexity of Fourier-based reconstruction in the first stage is $J\left(L\frac{K}{2}\log K + K\frac{L}{2}\log L\right) = \frac{1}{2}JKL(\log K + \log L)$, whereas the complexity in the second stage which recovers the fine-resolution pixels of Q coarse-resolution pixels is $KL(QJ \cdot N^2)^n$, yielding a total complexity of $\frac{1}{2}JKL(\log K + \log L) + KL\left(QJ \cdot N^2\right)^n$. For example, when $J = 8$, $K = 32$, $L = 32$, $N = 4$, $Q = 9$, and $n = 2$, the complexity for the direct sparse image reconstruction technique is 1.801×10^{16}, whereas that of the proposed second-stage technique is 1.359×10^9, which is a remarkable reduction from the former.

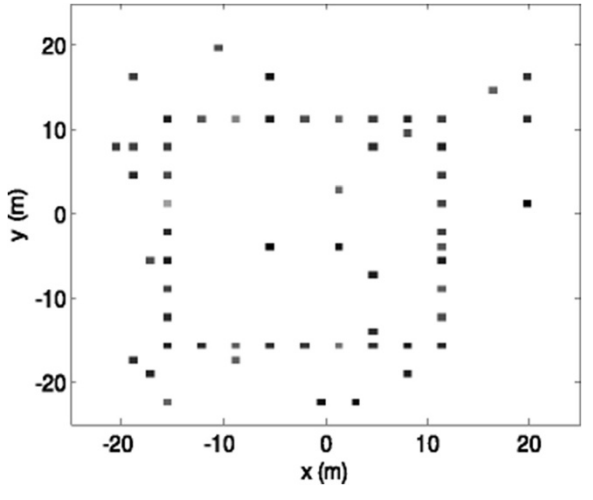

Figure 13 Image produced by the proposed two-stage image formation algorithm.

5 Simulation results

Simulations are performed to verify the effectiveness of the proposed technique. Assume that the passive radar system exploits a moving receiver to collect signals emitted from eight stationary illuminators and reflected in the scene of interest. The illuminators use respective frequencies and azimuth angles, as summarized Table 1, whereas the bandwidth of each signal is assumed to be 30 MHz. The receiver changes its azimuth angle from 10° to 20° during the observation period. The resulting wavenumber domain support is shown in Figure 8. Furthermore, we assume a sparse scene that consists of a collection of point targets, as shown in Figure 9, whose reflection coefficients follow an independent random complex Gaussian distribution. For each bi-static pair corresponding to an illuminator, the scattering coefficients are considered time-invariant during the observation because of the small azimuth angle of the receiver. The scattering coefficients, however, vary independently for bi-static pairs associated with different illuminators.

As a baseline for comparison, the result obtained from direct Fourier-based imaging is shown in Figure 10. Because of the inapplicability of coherent combination of the signals corresponding to different illuminators due to aspect-dependent target scattering, the sub-images obtained from the eight bi-static pairs are combined noncoherently. As we discussed earlier, Fourier transform suffers from several issues: The image resolution is limited by the poor Fourier resolution due to narrow signal bandwidth and small azimuth angles, whereas the grating lobe is high because of the sparse observation support in the wavenumber domain. It is evident from Figure 10 that the overall image resolution is undesirable due to these issues. We also show the results when conventional compressive sensing techniques, which do not consider the group sparsity, are used to reconstruct the image. Figure 11 depicts the noncoherently combined results of the eight sub-images that are individually constructed using the orthogonal matching pursuit (OMP) technique from the respective bi-static pairs to account for their different scattering coefficients. The performance degradation, particularly around the regions with dense scatterers, is evident in Figure 11.

In the proposed two-stage technique, we first obtain eight coarse-resolution images through the Fourier transform, as shown in Figure 12. It is clear from this figure that the image quality is poor because of the very low resolution. However, high-quality fine-resolution images are obtained by fusing the eight coarse-resolution images in the second stage through sparse image reconstruction. The results are shown in Figure 13, which recover the high-resolution pixels with a high fidelity.

6 Conclusions

In this paper, we have analyzed the signal characteristics in multi-static passive radar SAR and depicted the block sparsity of the sampling support in the wavenumber domain. Based on this property, an efficient two-stage image reconstruction technique is proposed. In this technique, the Fourier-based approach is used in the first stage to obtain coarse-resolution images separately for the signals emitted from each illuminator, whereas group sparsity-based approaches are used in the second stage to reconstruct a fine-resolution image. The proposed technique offers advantages over one-stage approaches: It yields substantial image quality improvement over the direct application of Fourier-based approaches to the observed data, whereas it achieves significant reduction of the computational complexity and comparable image quality when compared to direct application of group sparsity-based approaches to the observed data. The proposed technique permits effective consideration of illuminator-dependent scattering coefficients of the targets.

Endnote

[a]We recognize that there exist signals from earth observation SAR satellites, e.g., TerraSAR-X [5], that occupy a wide signal band at a high carrier frequency. However, this paper considers ground broadcast and wireless network signals that are typically narrowband.

Competing interests

The authors declare that they have no competing interests.

Acknowledgements

The work of XM is supported in part by the National Nature Science Foundation of China (Grant No. 61301210) and Nature Science Foundation of Jiangsu Province (Grant No. BK20130815).

Disclosure

Part of this work was presented at the 2014 IEEE Radar Conference [16].

Author details

[1]Department of Electronic Engineering, Nanjing University of Aeronautics and Astronautics, 29 Yudao St., Nanjing 210016, China. [2]Center for Advanced Communications, Villanova University, 800 E, Lancaster Ave., Villanova, PA 19085, USA.

Received: 2 March 2014 Accepted: 3 June 2014
Published: 8 July 2014

References

1. H Griffitths, N Long, Television-based bistatic radar. IEE Proc. Commun. Radar Signal Proc. **133**(7), 649–657 (1986)
2. CR Berger, B Demissie, J Hechkenbach, P Willett, S Zhou, Signal processing for passive radar using OFDM waveforms. IEEE J. Selected Topics Signal Proc. **4**(1), 226–238 (2010)
3. YD Zhang, B Himed, Moving target parameter estimation and SFN ghost rejection in multistatic passive radar, in *Proc. IEEE Radar Conf Ottawa, Canada*, ed. by (2013)
4. I Walterscheid, T Espeter, AR Brenner, J Klare, JHG Ender, H Nies, R Wang, O Loffeld, Bistatic SAR experiments with PAMIR and TerraSAR-X - setup, processing, and image results. IEEE Trans. Geosci. Rem. Sens. **48**(8), 3268–3279 (2010)

5. O Arikan, DC Munson, A tomographic formulation of bistatic synthetic aperture radar, in *Proc. Advances in Commun. Control Systems.* (Baton Rouge, LA, 1988), pp. 19–21
6. MD Desai, WK Jenkins, Convolution backprojection image reconstruction for spotlight mode synthetic aperture radar. IEEE Trans. Image Proc. **1**(4), 505–517 (1992)
7. V Krishnan, J Swoboda, CE Yarman, B Yazici, Multistatic synthetic aperture radar image formation. IEEE Trans. Image Proc. **19**(5), 1290–1306 (2010)
8. JL Walker, Range-doppler imaging of rotating objects. IEEE Trans. Aerosp. Electron. Syst. **AES-16**, 15–22 (1980)
9. Y Wu, DC Munson, Multistatic synthetic aperture imaging of aircraft using reflected television signals, in *Proc. SPIE Algorithms for Synthetic Aperture Radar Imagery VIII, vol. 4382*, 2001
10. DL Donoho, Compressed sensing. IEEE Trans. Inform. Theor. **52**(4), 1289–1306 (2006)
11. E Candes, J Romberg, T Tao, Robust uncertainty principles: exact signal reconstruction form highly incomplete frequency information. IEEE Trans. Inform. Theor. **52**(2), 489–509 (2006)
12. M Cetin, WC Karl, Feature-enhanced synthetic aperture radar image formation based on nonquadratic regularization. IEEE Trans. Image Proc. **10**(4), 623–631 (2001)
13. I Stojanovic, M Cetin, WC Karl, Compressed sensing of monostatic and multistatic SAR. IEEE Geosci Rem. Sens. Lett. **10**(6), 1444–1448 (2013)
14. Q Wu, YD Zhang, MG Amin, B Himed, Multi-static passive SAR imaging based on Bayesian compressive sensing, in *Proc. SPIE Compressive Sensing Conference.* (Baltimore, MD, 2014)
15. Q Wu, YD Zhang, MG Amin, F Ahmad, Through-the-wall radar imaging based on modified Bayesian compressive sensing, in *Proc. IEEE China Summit and International Conference on Signal and Information Processing.* (Xi'an, China, 2014)
16. X Mao, YD Zhang, MG Amin, MG Amin, Two-stage multi-static passive SAR imaging with reduced complexity, in *Proc. IEEE Radar Conf. Cincinnati, OH*, 2014
17. D Slepian, Prolate spheroidal wave functions, Fourier analysis and uncertainty-V: the discrete case. Bell Syst. Tech. J. **57**(5), 1371–1429 (1978)
18. S Qin, YD Zhang, Q Wu, MG Amin, Large-scale sparse reconstruction through partitioned compressive sensing, in Proc. Int. Conf. *Digital Signal Processing.* (Hong Kong, China, 2014)
19. JL Walker, Range-Doppler imaging of rotating objects. IEEE Trans. Aerosp. Electron. Syst. **AES-16**(1), 23–51 (1980)
20. CE Yonina, K Partick, B Helmut, Compressed sensing of block-sparse signals: uncertainty relations and efficient recovery. IEEE Trans. Signal Proc. **58**(6), 3042–3054 (2010)
21. S Ji, D Dunson, L Carin, Multitask compressive sensing. IEEE Trans. Signal Proc. **57**(1), 92–106 (2009)
22. Q Wu, YD Zhang, MG Amin, B Himed, Complex multitask Bayesian compressive sensing, in *Proc. IEEE Int. Conf. Acoust. Speech, Signal Proc. (ICASSP).* (Florence, Italy, 2014)
23. B Dror, BW Michael, FD Marco, S Shriram, GB Richard, Distributed compressed sensing of jointly sparse signals, in Proc. Asilomar Conf. *Signals, Systems and Computers.* (Pacific Grove, CA, 2005), pp. 1537–1541

doi:10.1186/1687-6180-2014-104
Cite this article as: Mao *et al.*: Low-complexity sparse reconstruction for high-resolution multi-static passive SAR imaging*. *EURASIP Journal on Advances in Signal Processing* 2014 **2014**:104.